Inorg. Chem. **2003**, *42*, 6729–6740

Solid State Coordination Chemistry: One-, Two-, and Three-Dimensional Materials Constructed from Molybdophosphonate Subunits Linked through Binuclear Copper Tetra-2-pyridylpyrazine Groups

Eric Burkholder,[†] Vladimir Golub,[‡] Charles J. O'Connor,[‡] and Jon Zubieta*,[†]

Department of Chemistry, Syracuse University, Syracuse, New York 13244, and University of New Orleans, New Orleans, Louisiana 70148

Received May 22, 2003

The hydrothermal reactions of MoO_3, an appropriate Cu(II) source, tetra-2-pyridylpyrazine (tpypyz), and phosphoric acid and/or an organophosphonate yielded a series of organic–inorganic hybrid materials of the copper-molybdophosphonate family. A common feature of the structures is the entrainment within the extended architectures of chemically robust $\{Mo_5O_{15}(O_3PR)_2\}^{4-}$ clusters as molecular building blocks. The cluster is a characteristic feature of the one-dimensional materials $[\{Cu_2(tpypyz)(H_2O)_3\}Mo_5O_{15}(HPO_4)(O_3PCH_2CO_2H)]\cdot H_2O$ (**1**·H_2O) and $[\{Cu_2(tpypyz)(H_2O)\}Mo_5O_{15}(O_3PC_6H_5)_2]\cdot 2H_2O$ (**2**·$2H_2O$), the two-dimensional network $[\{Cu_2(tpypyz)(H_2O)_3\}Mo_5O_{15}(HPO_4)_2]\cdot 2H_2O$ (**5**·$2H_2O$) and the three-dimensional frameworks $[\{Cu_2(tpypyz)(H_2O)_2\}Mo_5O_{15}\{O_3P(CH_2)_nPO_3\}]\cdot xH_2O$ [$n = 3$, $x = 2.25$ (**6**·$2.25H_2O$); $n = 4$, $x = 0.33$ (**7**·$0.33H_2O$)]. In the case of methylenediphosphonate as the phosphorus component, the unique chelating nature of the ligand precludes formation of the pentamolybdate core, resulting in the chain structures $[\{Cu_2(tpypyz)(H_2O)\}Mo_3O_8\ (HO_3PCH_2PO_3)_2]\cdot 8H_2O$ (**3**·$8H_2O$) and $[\{Cu_2(tpypyz)(H_2O)\}_2(Mo_3O_8)_2(O_3PCH_2PO_3)_3]\cdot 16.9H_2O$ (**4**·$16.9H_2O$). For structures **1**–**7**, the secondary metal–ligand building block is the binuclear $\{Cu_2(tpypyz)(H_2O)_x\}^{4+}$ cluster. There is considerable structural versatility as a result of the variability in the number of attachment sites at the phosphomolybdate clusters, the coordination geometry of the Cu(II), which may be four-, five-, or six-coordinate, the extent of aqua ligation, and the participation of phosphate oxygen atoms as well as molybdate oxo groups in bonding to the copper sites. Crystal data: **1**·H_2O, $C_{26}H_{28}N_6Cu_2Mo_5O_{28}P_2$, monoclinic $C2/c$, $a = 42.497(2)$ Å, $b = 10.7421(4)$ Å, $c = 20.5617(8)$ Å, $\beta = 117.178(1)°$, $V = 8350.1(5)$ Å^3, $Z = 8$; **2**·$2H_2O$, $C_{36}H_{32}N_6Cu_2Mo_5O_{24}P_2$, monoclinic $P2_1/c$, $a = 11.2478(7)$ Å, $b = 19.513(1)$ Å, $c = 21.063(1)$ Å, $\beta = 93.608(1)°$, $V = 4613.7(5)$ Å^3, $Z = 4$; **3**·$8H_2O$, $C_{26}H_{40}N_6Cu_2Mo_3O_{29}P_4$, monoclinic $C2/c$, $a = 32.580(2)$ Å, $b = 17.8676(9)$ Å, $c = 15.9612(8)$ Å, $\beta = 104.430(1)°$, $V = 8993.3(8)$ Å^3, $Z = 8$; **4**·$16.9H_2O$, $C_{51}H_{71.75}Cu_4Mo_6N_{12}O_{51}P_6$, monoclinic $P2_1/c$, $a = 27.929(3)$ Å, $b = 12.892(2)$ Å, $c = 22.763(3)$ Å, $\beta = 90.367(2)°$, $V = 8195.7(2)$ Å^3, $Z = 4$; **5**·$2H_2O$, $C_{24}H_{28}N_6Cu_2Mo_5O_{28}P_2$, monoclinic $P2_1/n$, $a = 11.3222(4)$ Å, $b = 18.7673(7)$ Å, $c = 19.4124(7)$ Å, $\beta = 98.819(1)°$, $V = 4076.1(3)$ Å^3, $Z = 4$; **6**·$2.25H_2O$, $C_{27}H_{28.5}N_6Cu_2Mo_5O_{24.25}P_2$, monoclinic $C2/c$, $a = 12.8366(5)$ Å, $b = 18.4221(8)$ Å, $c = 34.326(1)$ Å, $\beta = 100.546(1)°$, $V = 7980.1(6)$ Å^3, $Z = 8$; **7**·$^1/_3H_2O$, $C_{28}H_{28.7}N_6Cu_2Mo_5O_{23.3}P_2$, monoclinic $C2/c$, $a = 12.577(1)$ Å, $b = 18.336(1)$ Å, $c = 36.476(3)$ Å, $\beta = 91.929(2)°$, $V = 8407.3$ Å^3, $Z = 8$.

Introduction

The extensive contemporary interest in the properties and applications of inorganic oxides[1–4] has spurred significant activity in the design of synthetic phases. One approach to synthetically modified oxides exploits the structure-directing characteristics of organic molecules.[5–7] It is now recognized that even small amounts of organic components can dramati-

* Author to whom correspondence should be addressed. E-mail: jazubiet@syr.edu.
† Syracuse University.
‡ University of New Orleans.

(1) *Inorganic Materials*; Bruce, D. W., O'Hare, D., Eds.; Wiley: Chichester, 1992.
(2) *Modern Oxide Materials*; Cockayne, B., James, D. W., Eds.; Academic Press; New York, 1972.
(3) McCarroll, W. H. *Encyclopedia of Inorganic Chemistry*; King, R. B., Ed.; John Wiley & Sons: New York, 1994; Vol. 6, pp 2903−2946.
(4) Cheetham, A. K. *Science* **1964**, *264*, 794.

10.1021/ic030169o CCC: $25.00
Published on Web 09/25/2003

cally influence the structures of the inorganic oxide in the resultant composite materials. Furthermore, such organic−inorganic hybrid materials can combine appropriate organic and inorganic characteristics to provide novel structural types, as well as new properties arising from the interplay of the two components.[8] An alternative strategy for the "bottom-up" design of extended oxide materials relies on "self-assembly" from molecular cluster building blocks,[9,10] such as the extensive family of chemically robust polyoxometalates.[11,12]

Our synthetic strategy combines these methodologies by employing the organic component as a tether between discrete molecular oxide clusters in the design of extended structures.[13−16] However, in addition to the oxide clusters and organic ligand subunits that provide an anionic substructure, the multicomponent system also requires a charge-compensating component, which in our application is a secondary metal cation with a chelating organoamine ligand, which serves to fix a number of coordination sites on the secondary metal and dictate the availability of attachment sites to the oxide clusters. Consequently, the coordination complex cation that is assembled serves to provide charge-compensation, space-filling, passivating, and structure-directing roles. This interplay of the coordination preferences of the secondary metal site and the geometric constraints imposed by the ligands provides considerable structural flexibility as well as subunits for the spatial transmission of structural information.

Chart 1

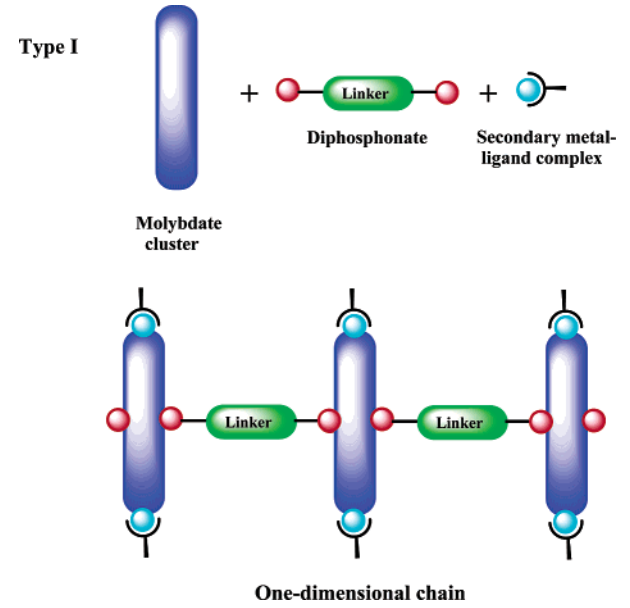

This general strategy has been demonstrated recently in our development of a class of materials constructed from the linking of molybdophosphonate clusters of the $[Mo_5O_{15}(O_3PR)_2]^{4-}$ type[17] through the expedient of tethering the $\{O_3P-\}$ groups through organic linkers. It is noteworthy that only in the presence of copper−organonitrogen complex cationic components as charge-compensating units were monophasic, crystalline materials obtained. These copper−ligand−molybdophosphonate materials were one-dimensional chains, with the copper−ligand subunits decorating the periphery of the oxide clusters. The design concept for these type I solids is illustrated in Chart 1. Structural manipulation may be readily accomplished by modifying the organophosphonate and/or the organonitrogen components. For example, introduction of a binucleating organonitrogen ligand offers the potential for tethering the clusters through the copper−ligand subunits. Thus, in the presence of a simple monopodal organophosphonate subunit, structural expansion can be achieved only through bridging via the binuclear copper−ligand moiety. However, as shown in Chart 2 for

(5) Stupp, S. I.; Braun, P. V. Science, **1997**, *277*, 1242 and references therein.
(6) Hagrman, P. J.; Hagrman, D.; Zubieta, J. *Angew. Chem., Int. Ed. Engl.* **1999**, *38*, 2639.
(7) Mitzi, D. B. *Prog. Inorg. Chem.* **1999**, *48*, 1.
(8) See for example: (a) Portier, J.; Choy, J.-H.; Subramamian, M. A. *Int. J. Inorg. Mat.* **2001**, *3*, 581. (b) Sanchez, C.; Soler-Illia, G. J. de A. A.; Ribot, F.; Lalot, T.; Mayer, C. R.; Calwil, V. *Chem. Mater.* **2001**, *13*, 3061 and references therein. (c) *Proceedings of the First European Workshop on Hybrid Organic−Inorganic Materials.* Sanchez, C., Ribot, F., Eds.; Special issue of *New J. Chem.* **1994**, *18*. (d) Davis, M. E.; Katz, A.; Ahmad, W. R. *Chem. Mater.* **1996**, *8*, 1820. (e) Evans, O. R.; Ngo, L.; Lin, W. B. *J. Am. Chem. Soc.* **2001**, *123*, 10395. (f) Sawaki, T.; Aoyama, Y. *J. Am. Chem. Soc.* **1999**, *121*, 4793. (g) Abrahams, B. E.; Jackson, P. A.; Robson, R. *Angew. Chem., Int. Ed.* **1998**, *37*, 2656. (h) Li, H.; Eddaoudi, M.; O'Keeffe, M.; Yaghi, O. M. *Nature* **1999**, *402*, 276. (i) Blanford, C. F.; Do, T. N.; Holland, B. T.; Stein, A. *Mater. Res. Soc. Symp. Proc.* **1999**, *549*, 61. (j) Carlucci, L.; Ciani, G.; Moret, M.; Proserpio, D. M.; Rizzato, S. *Angew. Chem., Int. Ed.* **2000**, 39, 1506. (k) Swift, J. A.; Ward, M. D. *Chem. Mater.* **2000**, *12*, 1501. (l) Chae, H. K.; Eddaoudi, M.; Kim, J.; Hauck, S. I.; Hartwig, J. F.; O'Keeffe, M.; Yaghi, O. M. *J. Am. Chem. Soc.* **2001**, *123*, 11482. (m) Zhao, H. R.; Heintz, A.; Ouyang, X.; Dunbar, K. R.; Campana, C. F.; Rogers, R. D. *Chem. Mater.* **1999**, *11*, 736.
(9) The concept of a molecular building block has been used previously as describing the application of small molecules in the design of nanoscale macromolecules and extended solids. The building block approach as related to the design of solids has been discussed in numerous reviews and reports: (a) Ferey, G., *J. Solid State Chem.* **2000**, *152*, 37. (b) Rao, C. N. R., *Proc. - Indian Acad. Sci., Chem. Sci.* **2001**. *113*, 363. (c) Weler, M. T. *J. Chem. Soc., Dalton Trans.* **2000**, 4227. (d) Fujita, M.; Umemoto, K.; Yoshizawa, M.; Fijita, N.; Kusukawa, T.; Biradhe, K. *Chem. Commun.* **2001**, 509. (e) Cotten, F. A.; Murillo, C. A. *Proc. Natl. Acad. Sci. U. S. A.* **2002**, *99*, 4810. (f) Eddaoudi, M.; Kim, J.; Vodak, D.; Sudik, A.; Wachter, J.; O'Keefe, M.; Yaghi, O. M. *Proc. Natl. Acad. Sci. U. S. A.* **2002**, *99*, 4900.
(10) The construction of extended structures from molecular cluster building blocks has received considerable attention. See for example: (a) DeBord, J. R. D.; Haushalter, R. C.; Meyer, L. M.; Rose, D. J.; Zapf, P. J.; Zubieta, J. *Inorg. Chim. Acta* **1997**, *256*,168. (b) Prohopuk, N.; Shriver, D. F. *Inorg. Chem.* **1997**, *36*, 5609. (c) Loose, I.; Bösing, M.; Klein, R.; Krebs, B.; Schulz, R. P.; Scharbert, B. *Inorg. Chim. Acta* **1997**, *263*, 99. (d) Khan, M. I.; Yobenn, G.; Doedens, R. J. *Angew. Chem., Int. Ed. Engl.* **1999**. *38*, 1292. (e) Liu, G.; Wei, Y.-G.; Liu, J.; Liu, Q.; Zhang, S.-W.; Tang, Y.-Q. *J. Chem. Soc., Chem. Commun.* **2000**, 1013. (f) Anokhina, E.; Day, C. S.; Essign, M. W.; Lachgan, A. *Angew. Chem., Int. Ed. Engl.* **2000**, *39*, 1047. (g) Yan, B.; Xu, Y.; Bu, Y.; Goh, N. K.; Chie, L. S.; Stucky, G. D. *J. Chem. Soc., Dalton Trans.* **2001**, 2009. (h) Schubert, U. *Chem. Mater.* **2001**, *13*, 3487. (i) Xu, B.; Wei, Y.; Barnes, C. L.; Peng, Z. *Angew. Chem., Int. Ed. Engl.* **2001**, *40*, 2290. (j) Niu, J.-Y.; Wu, Q.; Wang, J.-P. *J. Chem. Soc., Dalton Trans.* **2002**, 2512. (k) Shivaich, V.; Reddy, P. V. N.; Cronin, L.; Das, S. K. ? (l) Noland, B. K.; Selby, H. D.; Carducci, M. D.; Zhang, Z., *J. Am. Chem. Soc.* **2002**, *124*, 3222.
(11) Pope, M. T. *Heteropoly and Isopoly Oxometalates*; Springer: New York, 1983.
(12) *Polyoxometalate Chemistry*; Pope, M. T., Müller, A., Eds.; Kluwer Academic Press: The Netherlands, 2001.
(13) Finn, R. C.; Burkholder, E.; Zubieta, J. *Chem. Commun.* **2001**, 1852.
(14) Burkholder, E.; Zubieta, J. *Chem. Commun.* **2001**, 2056.
(15) Finn, R. C.; Zubieta, J. *Inorg. Chem.* **2001**, *40*, 2466.
(16) Finn, R. C.; Burkholder, E.; Zubieta, J. *Inorg. Chem.* **2002**, *41*, 2109.
(17) Kwak, W.; Pope, M. T.; Scully, T. F. *J. Am. Chem. Soc.* **1975**, *97*, 5735.

Chart 2

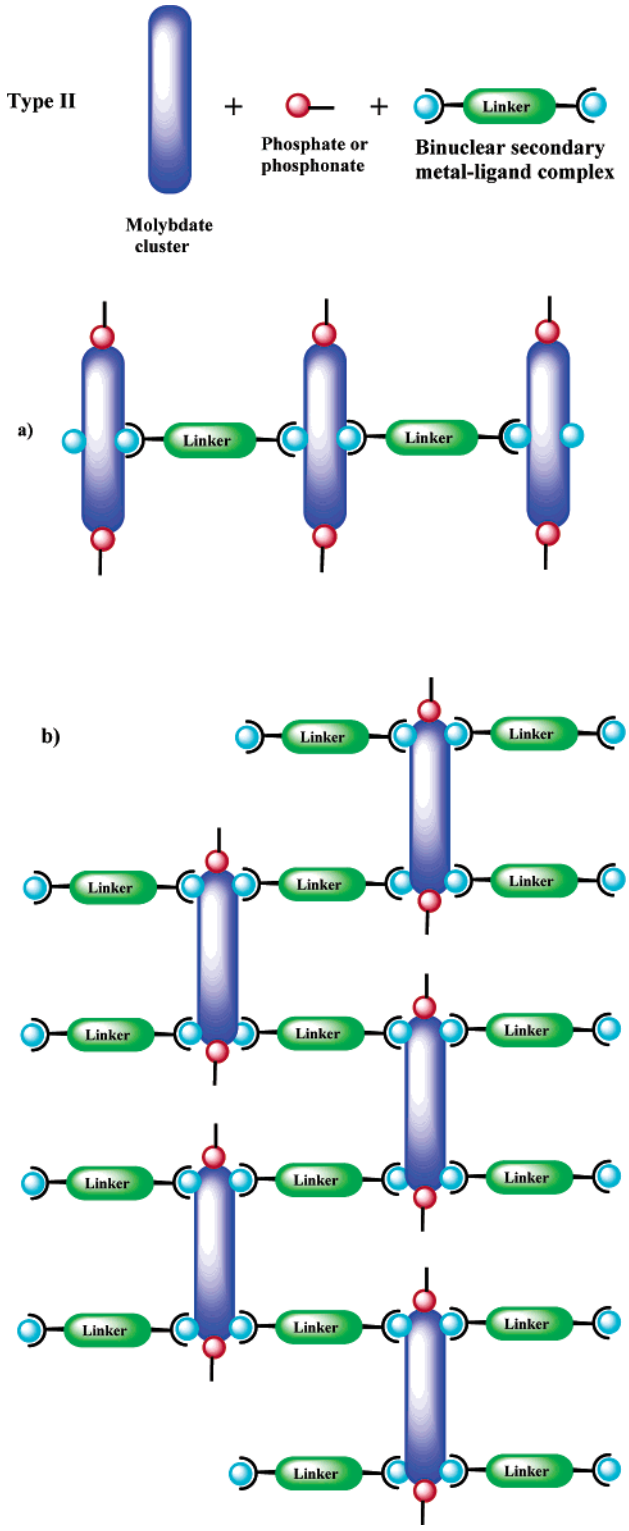

Chart 3

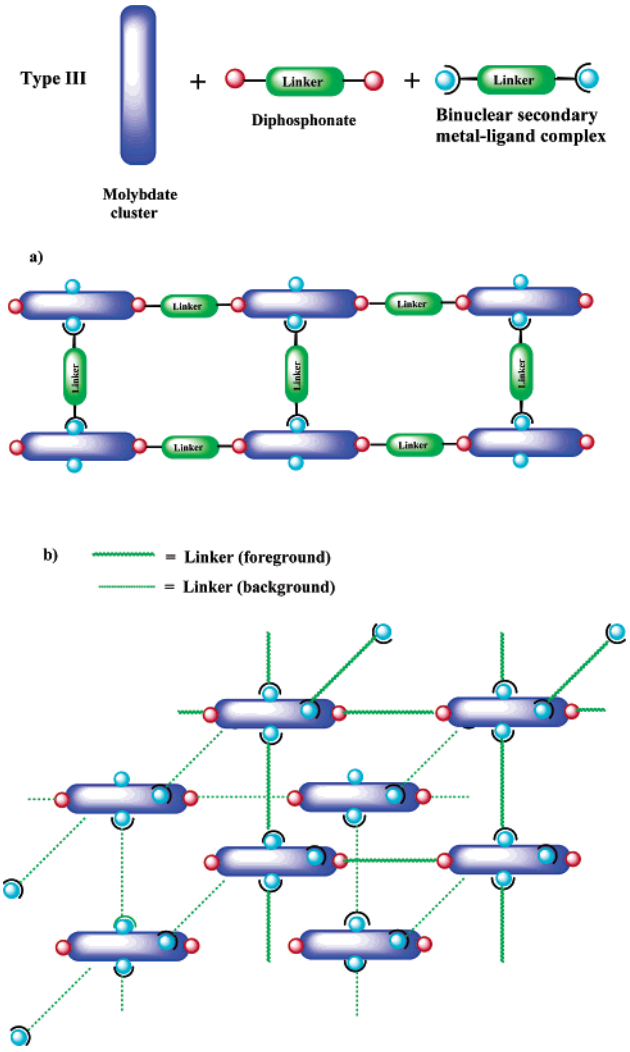

type II materials, the resultant dimensionality depends on the number of points of attachment available on the surface of the molybdophosphonate cluster. Previous experience suggests that two, three, or four Mo−O−Cu linkages may be established, potentiating the design of one- or two-dimensional materials. Finally, the combination of diphosphonate tethers and binuclear copper−organonitrogen subunits offers the possibility of two- or three-dimensional architectures, depending on the number of attachment sites occupied on the surface of the pentamolybdate cluster (type III materials of the Chart 3). In this study, we report the preparation and structures of a series of copper−molybdophosphonates, exploiting the binucleating ligand tetra-2-pyridylpyrazine (tpypyz) to provide the $\{Cu_2(tpypyz)\}^{4+}$ complex cationic building block. Depending on the identity of the phosphorus component and the reaction conditions, one-dimensional $[\{Cu_2(tpypyz)(H_2O)_3\}Mo_5O_{15}(HPO_4)(O_3PCH_2CO_2H)]\cdot H_2O$ (**1**·H_2O), $[\{Cu_2(tpypyz)(H_2O)\}Mo_5O_{18}(O_3PC_6H_5)_2]\cdot 2H_2O$ (**2**·$2H_2O$), $[\{Cu_2(tpypyz)(H_2O)\}Mo_3O_8(HO_3PCH_2PO_3)_2]\cdot 8H_2O$ (**3**·$8H_2O$), and $[\{Cu_2(tpypyz)(H_2O)\}_2(Mo_3O_8)_2(O_3PCH_2PO_3)_3]\cdot 16.9H_2O$ (**4**·$16.9H_2O$); two-dimensional $[\{Cu_2(tpypyz)(H_2O)_3\}Mo_5O_{15}(HPO_4)_2]\cdot 2H_2O$ (**5**·$2H_2O$); and three-dimensional $[\{Cu_2(tpypyz)(H_2O)_2\}Mo_5O_{15}\{O_3P(CH_2)_nPO_3\}]\cdot xH_2O$ [$n = 3$, $x = 2.25$ (**6**·$2.25H_2O$); $n = 4$, $x = 0.33$ (**7**·$0.33H_2O$)] materials have been prepared.

Experimental Section

General Considerations. Chemicals were used as obtained without further purification with the exception of butylenediphosophonic acid and 1,4-diphosphonobenzene, which were synthesized by the reported methods.[18,19] Copper(II) acetate monohydrate,

(18) Arnold, D. I.; Ouyang, X.; Clearfield, A. *Chem. Mater.* **2002**, *14*, 2020.

copper(II) sulfate pentahydrate, tetra-2-pyridinylpyrazine (tpyprz), phenylphosphonic acid, and phosphonoacetic acid were purchased from Aldrich; acetic acid, hydrofluoric acid (41−51% HF), and sulfuric acid were purchased from Acros; molybdenum(VI) oxide 99.5%, methlylenediphosphonic acid, and proplyenediphosphonic acid were purchased from Alfa Aesar. All syntheses were carried out in 23-mL poly(tetrafluoroethylene)-lined stainless steel containers under autogenous pressure. The reactants were stirred briefly, and the initial pH was measured before heating. Water was distilled above 3.0 MΩ in house using a Barnstead model 525 Biopure Distilled Water Center. The initial and final pHs of the reactions were measured using Hydrion pH sticks.

Synthesis of [{Cu_2(tpypyz)(H_2O)$_3$}Mo_5O_{15}(HPO_4)($O_3PCH_2CO_2H$)]·H_2O (1·H_2O). The reaction of MoO_3 (0.189 g, 1.313 mmol), $CuSO_4$·$5H_2O$ (0.131 g, 0.525 mmol), tpypyz (0.104 g, 0.268 mmol), $H_2PO_3CH_2CO_2H$ (0.096 g, 0.686 mmol), H_2O (10.10 g, 560 mmol), and concentrated H_2SO_4 (0.162 g) in the mole ratio 4.90:1.96:1.00:2.56:2090 at 125 °C for 48.5 h yielded yellow crystals of **1**·H_2O in 65% yield that were suitable for X-ray diffraction: initial pH, 1.5; final pH, 1.0. IR (KBr pellet, cm^{-1}): 3447 (m), 1647 (w), 1560 (w), 1420 (w), 1215 (m), 1128 (m), 936 (s), 909 (s), and 699 (s).

Synthesis of [{Cu_2(tpypyz)(H_2O)}Mo_5O_{15}($O_3PC_6H_5$)$_2$]·$2H_2O$ (2·$2H_2O$). A solution of MoO_3 (0.176 g, 1.222 mmol), $Cu(CH_3CO_2)_2$·H_2O (0.103 g, 0.516 mmol), tpypyz (0.085 g, 0.219 mmol), $C_6H_5PO(OH)_2$ (0.173 g, 1.218 mmol), and H_2O (10.18 g, 565 mmol) in the mole ratio 5.58:2.36:1.00:5.56:2580 was stirred briefly before heating to 150 °C for 96 h: initial pH, 1.5; final pH, 1.5. Dark-yellow crystals of **2**·$2H_2O$, suitable for X-ray studies, were isolated in 35% yield. IR (KBr pellet, cm^{-1}): 3448 (m), 1654 (w), 1560 (w), 1420 (w), 1127 (w), 1053 (m), 972 (w), 933 (s), 905 (s), 705 (s), and 565 (w).

Synthesis of [{Cu_2(tpypyz)(H_2O)}Mo_3O_8($HO_3PCH_2PO_3$)$_2$]·$8H_2O$ (3·$8H_2O$). The reaction of MoO_3 (0.176 g, 1.222 mmol), $Cu(CH_3CO_2)_2$·H_2O (0.100 g, 0.501 mmol), tpypyz (0.085 g, 0.219 mmol), $H_2PO_3CH_2PO_3H_2$ (0.109 g, 0.865 mmol), H_2O (10.19 g, 565 mmol), and CH_3CO_2H (0.229 g) in the mole ratio 5.58:2.29:1.00:3.95:2580 at 180 °C for 49.5 h gave dark-yellow crystals of **3**·$8H_2O$ in 53% yield: initial pH, 1.5; final pH, 1.5. IR (KBr pellet, cm^{-1}): 3751 (m), 3422 (s), 1718 (w), 1647 (m), 1560 (m), 1474 (w), 1420 (w), 1162 (m), 1044 (s), 912 (s), 785 (w), 649 (m), and 555 (m).

Synthesis of [{Cu_2(tpypyz)(H_2O)}$_2$(Mo_3O_8)$_2$($O_3PCH_2PO_3$)$_3$]·$16.9H_2O$ (4·$16.9H_2O$). A solution of MoO_3 (0.109 g, 0.757 mmol), $Cu(CH_3CO_2)_2$·H_2O (0.099 g, 0.496 mmol), tpypyz (0.097 g, 0.250 mmol), $H_2PO_3CH_2PO_3H_2$ (0.071 g, 0.563 mmol), H_2O (10.030 g, 557 mmol), and CH_3CO_2H (0.0.201 g) in the mole ratio 3.03:1.98:1.00:2.25:2228 at 180 °C for 48 h yielded yellow crystals of **4**·$14.8H_2O$ isolated in a 90% yield that were suitable for X-ray diffraction: initial pH, 1.5; final pH, 1.5. IR (KBr pellet, cm^{-1}): 3422 (b), 1637 (w), 1600 (w), 1477 (m), 1422 (m), 1163 (s), 1023 (s), 926 (s), 905 (s), 811 (w), 786 (w), 745 (m), 650 (s), and 567 (m).

Synthesis of [{Cu_2(tpypyz)(H_2O)$_3$}Mo_5O_{15}(HPO_4)$_2$]·$2H_2O$ (5·$2H_2O$). A mixture of MoO_3 (0.190 g, 1.320 mmol), $Cu(CH_3CO_2)_2$·H_2O (0.102 g, 0.511 mmol), tpypyz (0.102 g, 0.263 mmol), 1,4-diphosphonobenzene (0.157 g, 0.659 mmol), H_2O (10.022 g, 556 mmol), and concentrated H_2SO_4 in the mole ratio 5.02:1.94:1.00:2.51:2114 was stirred briefly before heating to 150 °C for 48.5 h. Green crystals of **5**·$2H_2O$ were isolated in 72% yield: initial pH, 1.5; final pH, 1.0. IR (KBr pellet, cm^{-1}): 3421 (s), 1654 (w), 1601 (w), 1475 (w), 1420 (m), 1216 (m), 1113 (m), 1029 (m), 965 (m), 939 (s), 918 (s), 782 (w), 702 (s), 607 (w), 570 (w), and 419 (w).

Synthesis of [{Cu_2(tpypyz)(H_2O)$_2$}Mo_5O_{15}{$O_3P(CH_2)_3PO_3$}]·$2.25H_2O$ (6·$2.25H_2O$). A solution of MoO_3 (0.160 g, 1.112 mmol), $Cu(CH_3CO_2)_2$·H_2O (0.089 g, 0.446 mmol), tpypyz (0.086 g, 0.221 mmol), $H_2PO_3(CH_2)_3PO_3H_2$ (0.092 g, 0.451 mmol), and H_2O (10.03 g, 557 mmol) in the mole ratio 5.03:2.02:1.00:2.04:2520 was stirred briefly before heating to 150 °C for 48.5 h. Dark-green crystals of **6**·$2.25H_2O$ suitable for X-ray diffraction were isolated in 70% yield: initial pH, 2.5; final pH, 1.5. IR (KBr pellet, cm^{-1}): 3488 (s), 1654 (w), 1597 (m), 1470 (m), 1419 (m), 1263 (w), 1203 (w), 1116 (s), 1031 (s), 973 (s), 920 (s), 888 (s), 859 (s), 785 (m), 693 (s), 573 (w), and 414 (w).

Synthesis of [{Cu_2(tpypyz)(H_2O)$_2$}Mo_5O_{15}{$O_3P(CH_2)_4PO_3$}]·$0.33H_2O$ (7·$0.33H_2O$). The reaction of MoO_3 (0.160 g, 1.112 mmol), $Cu(CH_3CO_2)_2$·H_2O (0.090 g, 0.451 mmol), tpypyz (0.087 g, 0.224 mmol), $H_2PO_3(CH_2)_4PO_3H_2$ (0.096 g, 0.440 mmol), H_2O (10.03 g, 557 mmol), and HF (0.215 g) in the mole ratio 4.96:2.01:1.00:1.96:2487 at 150 °C for 72 h provided dark-green crystals of **7**·$0.33H_2O$ in 60% yield: initial pH, 1.5; final pH, 1.0. IR (KBr pellet, cm^{-1}): 3752 (m), 3448 (s), 1718 (w), 1654 (m), 1596 (w), 1560 (m), 1474 (w), 1420 (w), 1138 (m), 1036 (w), 973 (w), 913 (s), 790 (m), 668 (s), 570 (w), and 422 (w).

X-ray Crystallography. Structural measurements for **1**−**7** were performed on a Bruker-AXS SMART-CCD diffractometer at low temperature (87−90 K) using graphite-monochromated Mo Kα radiation ($\lambda_{MoK\alpha}$ = 0.71073 Å).[20] The data were corrected for Lorentz and polarization effects and absorption using SADABS.[21] The structures were solved by direct methods. In all cases, all non-hydrogen atoms were refined anisotropically. After all of the non-hydrogen atoms were located, the models were refined against F^2, initially using isotropic and later anisotropic thermal displacement parameters. Hydrogen atoms were introduced in calculated positions and refined isotropically. Neutral atom scattering coefficients and anomalous dispersion corrections were taken from the *International Tables*, Vol. C. All calculations were performed using SHELXTL crystallographic software packages.[22]

Crystallographic details for the structures of **1**−**7** are summarized in Table 1. Atomic positional parameters, full tables of bond lengths and angles, and anisotropic temperature factors are available in the Supporting Information. The metrical parameters for **1**−**7** are unexceptional and, consequently, are not tabulated in the printed paper.

Magnetism. Magnetic data were recorded on 17−25 mg samples of compound in the 2−300 K temperature range using a Quantum Design MPMS-5S SQUID spectrometer. Calibrating and operating procedures have been reported previously.[23] The temperature-dependent data were obtained at a magnetic field of H = 1000 Oe.

Thermal Gravimetric Analyses. Thermogravimetric studies were performed using 10−20 mg samples in an Auto TGA 2950HR instrument under a 50 mL/min flow of synthetic air. The temperature was ramped from 20 to 650 °C at a rate of 5 °C/min for the decomposition processes and 1 °C/min for the dehydrations.

Results and Discussion

Synthesis and Infrared Spectroscopy. The copper−molybdophosphonates **1**−**7** were prepared using conventional

(19) Medoukali, Mutin, P. H.; Vioux, A. *J. Mater. Chem.* **1999**, *9*, 2553.

(20) *SMART Software Reference Manual*; Siemens Analytical X-ray Instruments, Inc.: Madison, WI, 1994.

(21) Sheldrick, G. M. *SADABS: Program for Empirical Absorption Corrections*; University of Göttingen: Göttingen, Germany, 1996.

(22) Sheldrick, G. M. *SHELXTL96: Program for Refinement of Crystal Structures*; University of Gottingen: Göttingen, Germany, 1996.

(23) O'Connor, C. J. *Prog. Inorg. Chem.* **1979**, *29*, 203.

Table 1. Summary of Crystallographic Data for the Structures of $[\{Cu_2(tpyprz)(H_2O)_3\}Mo_5O_{15}(HPO_4)(O_3PCH_2CO_2H)]\cdot H_2O$ (**1**·H_2O), $[\{Cu_2(tpyprz)(H_2O)\}Mo_5O_{15}(O_3PC_6H_5)_2]\cdot 2H_2O$ (**2**·$2H_2O$), $[\{Cu_2(tpyprz)(H_2O)\}Mo_3O_8(HO_3PCH_2PO_3)_2]\cdot 8H_2O$ (**3**·$8H_2O$), $[\{Cu_2(tpyprz)(H_2O)\}_2(Mo_3O_8)_2(O_3PCH_2PO_3)_3]\cdot 16.9H_2O$ (**4**·$16.9H_2O$), $[\{Cu_2(tpyprz)(H_2O)_3\}Mo_5O_{15}(HPO_4)_2]\cdot 2H_2O$ (**5**·$2H_2O$), $[\{Cu_2(tpyprz)(H_2O)_2\}Mo_5O_{15}\{O_3P(CH_2)_3PO_3\}]\cdot 2.25H_2O$ (**6**·$2.25H_2O$), and $[\{Cu_2(tpyprz)(H_2O)_2Mo_5O_{15}\{O_3P(CH_2)_4PO_3\}]\cdot 0.33H_2O$ (**7**·$0.33H_2O$)

	1·H_2O	**2**·$2H_2O$	**3**·$8H_2O$	**4**·$16.9H_2O$	**5**·$2H_2O$	**6**·$2.25H_2O$	**7**·$0.33H_2O$
empirical formula	$C_{26}H_{28}N_6Cu_2Mo_5O_{28}P_2$	$C_{36}H_{32}N_6Cu_2Mo_5O_{24}P_2$	$C_{26}H_{40}N_6Cu_2Mo_3O_{29}P_4$	$C_{51}H_{71.8}N_{12}Cu_4Mo_6O_{50.9}P_6$	$C_{24}H_{28}N_6Cu_2Mo_5O_{28}P_2$	$C_{27}H_{28.5}N_6Cu_2No_5O_{24.25}P_2$	$C_{28}H_{28.67}N_6Cu_2Mo_5O_{23.33}P_2$
fw	1541.26	1601.40	1439.42	2683.02	1517.24	1493.78	1491.30
cryst syst	monoclinic	monoclinic	monoclinic	monoclinic	monoclinic	monoclinic	monoclinic
space group	*C*2/*c*	*P*2$_1$/*c*	*C*2/*c*	*P*2$_1$/*c*	*P*2$_1$/*n*	*C*2/*c*	*C*2/*c*
a, Å	42.497(2)	11.2478(7)	32.580(2)	27.929(3)	11.3222(4)	12.8366(5)	12.577(1)
b, Å	10.7421(4)	19.513(1)	17.8676(9)	12.892(2)	18.7673(7)	18.4221(8)	18.336(1)
c. Å	20.5617(8)	21.063(1)	15.9612(8)	22.763(3)	19.4124(7)	34.326(1)	36.476(3)
β, deg	117.178(1)	93.608(1)	104.430(1)	90.367(2)	98.819(1)	100.546(1)	91.929(2)
V, Å^3	8350.1(5)	4613.7(5)	8998.3(8)	8195.7(2)	4076.1(3)	7980.1(6)	8407.3(1)
Z	8	4	8	4	4	8	8
D_{calcd}, g cm^{-3}	2.452	2.305	2.125	2.174	2.472	2.487	2.356
μ, mm^{-1}	2.637	2.385	1.990	2.133	2.699	2.748	2.607
T, K	90(2)	88(2)	90(2)	90(2)	90(2)	87(2)	89(2)
λ, Å	0.71073	0.71073	0.71073	0.71073	0.71073	0.71073	0.71073
R1[a]	0.0766	0.0765	0.1009	0.0676	0.0641	0.0659	0.1018
wR2[b]	0.1031	0.1256	0.1465	0.1258	0.0907	0.0992	0.1161

[a] $R1 = \Sigma||F_o| - |F_c||/\Sigma|F_o|$. [b] $wR2 = \{\Sigma[w(F_o^2 - F_c^2)^2]/\Sigma[w(F_o^2)^2]\}^{1/2}$.

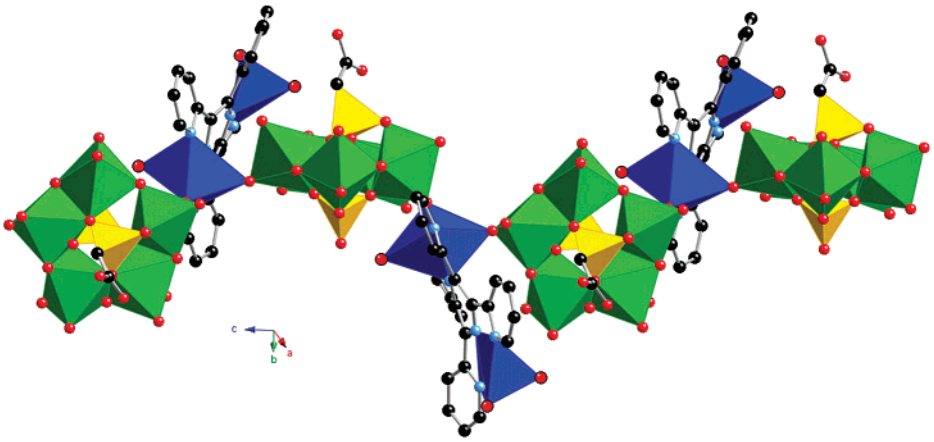

Figure 1. A view of the one-dimensional structure of $[\{Cu_2(tpypyz)(H_2O)_3\}Mo_5O_{15}(HPO_4)(O_3PCH_2CO_2H)]\cdot H_2O$ (**1**·H_2O).

hydrothermal methods. In contrast to high-temperature solid-state syntheses, which may not allow retention of the structural characteristics of organic starting materials, "chimie douce" techniques, such as cation exchange, intercalation, sol−gel, and hydrothermal methods may be exploited in the preparation of organic−inorganic hybrid materials.[24,25] The isolation of two structurally distinct products **3** and **4** for the methyldiphosphonate derivatives illustrates the common observation that relatively small changes in hydrothermal reaction conditions can have profound structural consequences. It is noteworthy that the arylphosphonates, 1,4-diphosphonobenzene and $H_2O_3PCH_2CO_2H$, decompose under hydrothermal conditions to produce phosphate, as noted for **1**·H_2O and **5**·$2H_2O$. Curiously, while several attempts were made to prepare **5** directly from H_3PO_4, in the absence of 1,4-diphosphonobenzene, these were unsuccessful, suggesting a structure-directing role for the diphosphonate or its monophosphonate decomposition product.

The infrared spectra of the complexes are characterized by strong bands in the 900−936 cm^{-1} range, attributed to υ(Mo═O), and medium to strong bands in the 675−725 cm^{-1} range, associated with υ(Mo−O−Mo). The medium to strong peaks in the 960−1160 cm^{-1} range are attributed to υ(P−O) bands of the organophosphonate ligands, while the prominent bands in the 1400−1650 cm^{-1} region are assigned to the tpypyz ligand.

X-ray Structures. The structural chemistry of the materials constructed from $\{Cu_2(tpypyz)\}^{4+}$ cationic building block linking molybdophosphonate subunits exhibits considerable variety, manifested by one-, two-, and three-dimensional architectures. The chain structures of $[\{Cu_2(tpypyz)(H_2O)_3\}Mo_5O_{15}(HPO_4)(O_3PCH_2CO_2H)]\cdot H_2O$ (**1**·H_2O) and $[\{Cu_2(tpypyz)(H_2O)\}\ Mo_5O_{15}(O_3PC_6H_5)_2]\cdot 2H_2O$ (**2**·$2H_2O$) are characteristic of materials constructed from the cationic $\{Cu_2(tpypyz)(H_2O)_x\}^{4+}$ and the anionic $\{Mo_5O_{15}(RPO_3)_2\}^{4-}$ cluster building blocks.

As illustrated in Figure 1, the structure of **1** consists of sinusoidal chains of $\{Mo_5O_{15}(HPO_4)(O_3PCH_2CO_2H)\}^{4-}$ clusters linked through $\{Cu_2(tpypyz)(H_2O)_3\}^{4+}$ binuclear units. The molybdophosphonate cluster exhibits the characteristic structure based on a pentanuclear ring of edge- and corner-sharing $\{MoO_6\}$ octahedra, capped above and below by

(24) Livage, J. *Chem. Scr.* **1988**, *28*, 9.
(25) Rouxel, J. *Chem. Scr.* **1988**, *28*, 33.

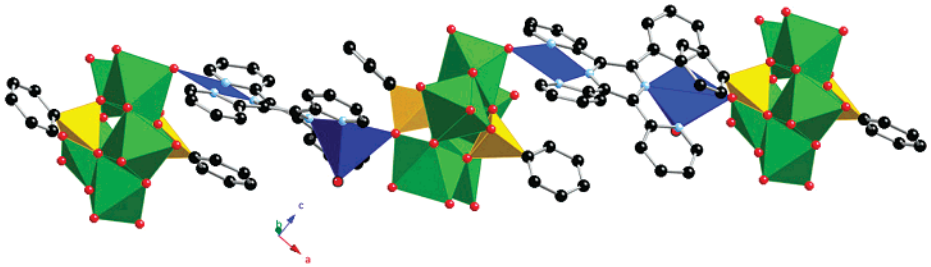

Figure 2. Polyhedral representation of the structure of $[\{Cu_2(tpypyz)(H_2O)\}Mo_5O_{15}(O_3PC_6H_5)_2]\cdot 2H_2O$ (**2**·$2H_2O$).

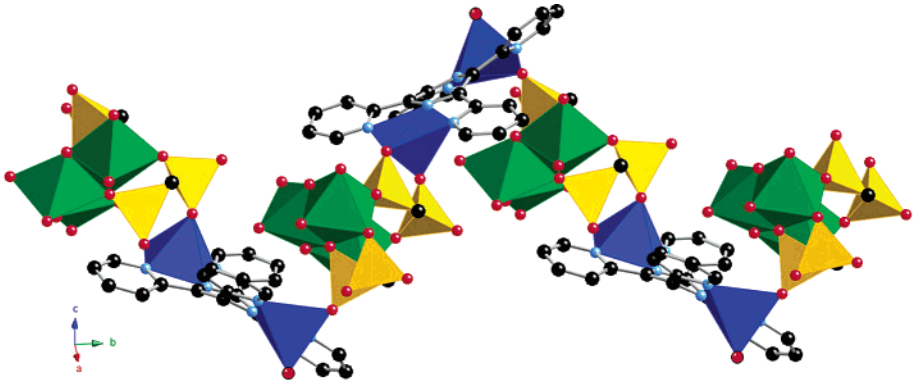

Figure 3. A view of the one-dimensional structure of $[\{Cu_2(tpypyz)(H_2O)\}Mo_3O_8(HO_3PCH_2PO_3)_2]\cdot 8H_2O$ (**3**·$8H_2O$).

RPO_3^{n-} units (R = −OH and $-CH_2CO_2H$), each sharing three vertexes with the central ring. The unusual feature of this structure is the association of two distinct phosphorus subunits within the phosphomolybdate substructure. To our knowledge, this is the first example of such a cluster bearing different phosphorus components.

It is also noteworthy that the $\{Cu_2(tpypyz)(H_2O)_3\}^{4+}$ unit adopts a rather unusual bridging mode. Rather than extending the structure through connectivity at both Cu(II) sites, a single copper site bridges adjacent phosphomolybdate clusters. While this copper site exhibits "4 + 2" Jahn−Teller distorted geometry through coordination to three ligand nitrogen donors, two oxo-groups, and a water molecule, the second copper center exhibits square pyramidal coordination, defined by the three ligand nitrogen atoms and two aqua ligands. This second copper site projects into the interchain domain and nestles in the cavity produced by the ruffling of the adjacent chain.

There is significant hydrogen bonding between the carboxylate groups of one chain and the aqua ligand of the octahedral copper site of an adjacent chain, producing a hydrogen-bonded network of chains in the *bc* plane.

The structure of **2**·$2H_2O$ is also one-dimensional, constructed from $\{Mo_5O_{15}(O_3PC_6H_5)_2\}^{4-}$ clusters and $\{Cu_2(tpypyz)(H_2O)\}^{4+}$ subunits, as shown in Figure 2. In contrast to the structure of **1**, the binuclear copper building block adopts the more common role of extender, propagating the chain structure through coordination at both Cu(II) sites. Thus, while the distance between the centroids of the phosphomolybdate clusters in **1** is 10.9 Å, the corresponding distance in **2** is 14.9 Å. A curious feature of the structure is the presence of two distinct Cu(II) geometries, one the common square pyramidal geometry (three nitrogen donors, one oxo-group, and an axial aqua ligand) and the second a unique example in the structural chemistry of this family of compounds of a square planar site (three nitrogen donors and an oxo group). The structural versatility of the copper subunit is quite evident in comparing the structures of **1** and **2**, where four "4 + 1" and 4 + 2 coordination modes are manifested.

The third one-dimensional structure is manifested by $[\{Cu_2(tpypyz)(H_2O)\}Mo_3O_8(HO_3PCH_2PO_3)_2]\cdot 8H_2O$ (**3**·$8H_2O$), shown in Figure 3. In this case, the structure is constructed from $\{Mo_3O_8(HO_3PCH_2PO_3)_2\}^{4-}$ clusters linked through $\{Cu_2(tpypyz)(H_2O)\}^{4+}$ subunits. The unusual phosphomolybdate core of the structure is constructed from a triad of edge-sharing $\{MoO_6\}$ octahedra, which bonds to two $\{HO_3PCH_2PO_3\}^{3-}$ ligands through three oxygen donors to each.

Each methylenediphosphonate ligand bonds to two molybdates of the triad through two oxygen donors on one phosphorus terminus and to the third Mo site through an oxygen on the second phosphorus. One methylenediphosphonate group also chelates to a copper site through oxygen donors on each phosphorus atom to produce a {O−P−O−Cu−O−P} chelate ring, while the second engages in a single link to the other copper site. Consequently, the first methylenephosphonate group possesses a single pendant {P−OH} unit, whereas the second projects two pendant {P═O} groups into the interchain domain.

The copper sites of the $\{Cu_2(tpypyz)H_2O\}^{4+}$ subunit of **3** are again inequivalent. In this instance, one site is square pyramidal, bonding to three nitrogen donors and two oxygens from a diphosphonate ligand, while the second site bonds to three nitrogen donors, an oxygen from the second diphosphonate ligand, and an aqua ligand. A curious feature of the structure is the absence of any Mo−O−Cu bridging interactions. Chain extension is accomplished exclusively through

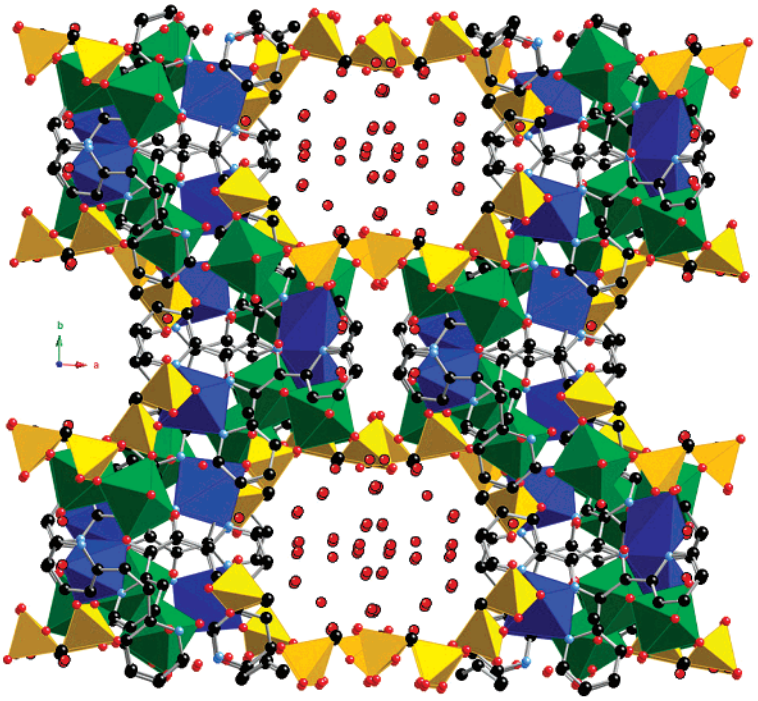

Figure 4. A view of the packing of adjacent chains in **3** to produce large, water-containing cavities in the *ab* plane.

Cu−phosphonate oxygen linkages, a unique example of this modality for this family of materials.

The chain of **3** is distinctly ruffled, propagating in a sinusoidal manner with an amplitude of 7.0 Å and a period of 17.9 Å. In the *ab* plane projection, adjacent chains are oriented so as to direct one phosphorus tetrahedron toward an adjacent chain, producing virtual channels defined by 14 phosphate tetrahedra of dimensions 9.0 Å × 12.5 Å. These channels, as shown in Figure 4, are occupied by water molecules of crystallization. The entrainment of ca. 10% water by weight reflects the considerable "void" volume associated with the structure.

The other methylenediphosphonate derivative of this study, $[\{Cu_2(tpypyz)(H_2O)\}_2(Mo_3O_8)_2(O_3PCH_2PO_3)_3]\cdot 16.9H_2O$ (**4**·16.9H_2O), is also a one-dimensional chain, as shown in Figure 5. The structure is constructed of unique $\{(Mo_3O_8)_2(O_3PCH_2PO_3)_3\}^{8-}$ clusters, linked through $\{Cu_2(tpypyz)(H_2O)\}^{4+}$ subunits into a spiral chain. The molybdophosphonate cluster, shown in Figure 5b, consists of two molybdate triads, each characterized by a central $\{MoO_6\}$ octahedron sharing cis edges with the peripheral $\{MoO_6\}$ octahedra. Each molybdate trinuclear unit bonds to one methylenediphosphonate group through three oxygen donors, leaving three available for copper coordination. The two trimolybdo-methylenediphosphonate moieties are linked through the third methylenediphosphonate ligand, which contributes three oxygen donors to each trinuclear molybdate cluster.

The Cu(II) sites link to these $\{(Mo_3O_8)_2(O_3PCH_2PO_3)_3\}^{8-}$ subunits exclusively through the phosphonate oxygen donors, that is, there are no Cu−O−Mo linkages through the oxo groups of the molybdates. Each of the two methylenediphosphonate groups associated with a single molybdate triad contributes its remaining three oxygen donors to copper coordination. Two oxygen atoms on adjacent phosphorus atoms engage in chelation to one Cu site, forming {Cu−O−P−C−P−O} six-membered rings, while the remaining oxygen donor links to another Cu site. Consequently, each of these methylenediphosphonate ligands links two $\{Cu_2(tpypyz)(H_2O)\}^{4+}$ subunits, and each $\{(Mo_3O_8)_2(O_3PCH_2PO_3)_3\}^{8-}$ cluster is associated with four $\{Cu_2(tpypyz)(H_2O)\}^{4+}$ subunits.

There are two distinct Cu(II) sites. One is square pyramidal with the basal plane defined by three nitrogen donors of the tpypyz ligand and an oxygen donor of the methylenediphosphonate and the apical position occupied by a second oxygen donor of the diphosphonate. The second site is also square pyramidal with the basal plane occupied by three nitrogen donors and an aqua ligand and the apical position by an oxygen donor from the methylenediphosphonate ligand.

As shown in Figure 5, the chain of **4** undulates with a period of 27.9 Å and an amplitude of 13.0 Å. When viewed parallel to the crystallographic *a* axis, the chain is distinctly seen to spiral, so as to form in projection a cavity of dimensions 4.0 Å × 6.5 Å. The spiral chains align along the *a* axis as shown in Figure 5c to produce cavities between chains, as well as cavities within the chains. This void volume is occupied by a significant amount of water of crystallization, ca. 9.9% by mass.

The structures of **3** and **4** both contain the $\{(Mo_3O_8)(O_3PCH_2PO_3)_2\}^{n-}$ subunit. However, in the case of **3**, both methylenediphosphonate linkers are bound to Cu(II) sites and singly protonated. In contrast, the $\{(Mo_3O_8)(O_3PCH_2PO_3)_2\}^{6-}$ subunit of **4** links to an additional $\{(Mo_3O_8)(O_3PCH_2PO_3)\}$ cluster through a methylenediphosphonate ligand associated with the molybdate sites in the chain propagation. The expanded $\{(Mo_3O_8)_2(O_3PCH_2PO_3)_3\}^{8-}$ cluster of **4** accom-

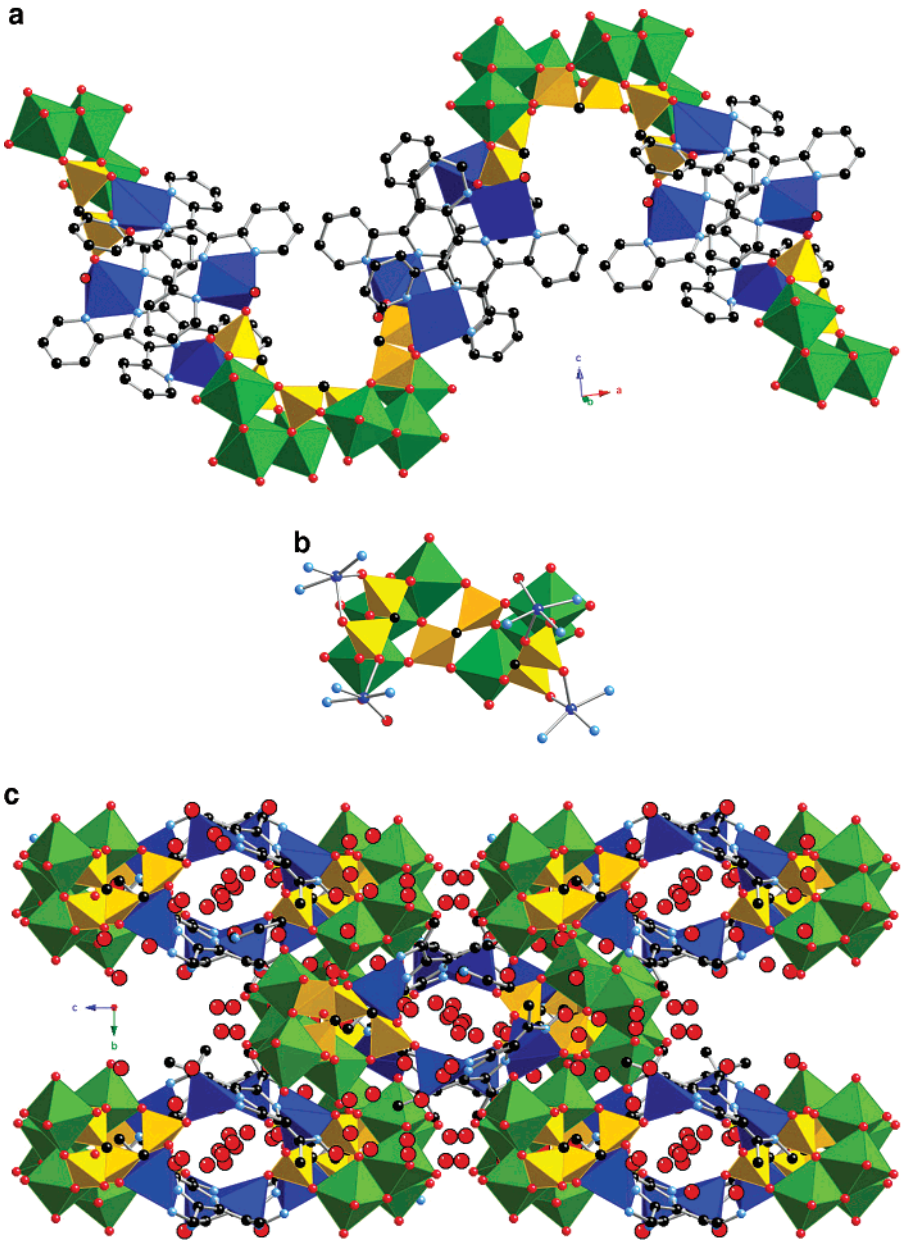

Figure 5. (a) The one-dimensional structure of $[\{Cu_2(tpypyz)(H_2O)\}_2(Mo_3O_8)_2(O_3PCH_2PO_3)_3]\cdot 14.8H_2O$ (**4**·$14.8H_2O$). (b) The $\{(Mo_3O_8)_2(O_3PCH_2PO_3)_3\}^{8-}$ subunit of **4**. (c) A projection onto the *bc* crystallographic plane of the packing of adjacent chains in **4** to produce both intrachain and interchain regions which accommodate water molecules of crystallization.

modates four peripheral Cu(II) sites, while the $\{(Mo_3O_8)(HO_3PCH_2PO_3)_2\}^{4-}$ subunit of **3** associates with two Cu(II) sites.

It is also noteworthy that in contrast to the structures of **1** and **2**, the structures of **3** and **4** are not constructed from the common $\{Mo_5O_{15}(RPO_3)_2\}^{4-}$ building block. While the $\{Mo_5O_{15}(RPO_3)_2\}^{4-}$ and $\{Mo_6O_{18}(RAsO_3)_2\}^{4-}$ building blocks are a common feature of the Mo/O/E/copper−organonitrogen hybrid phases as noted in Table 2, there are a growing number of examples which are constructed from other $\{Mo_xO_y(O_3ER)_3\}^{n-}$ building blocks, as noted in the table. It is apparent that the majority of these latter structure types contain methylenediphosphonate as a component. The absence of the $\{Mo_5O_{15}(RPO_3)_2\}^{4-}$ building block in these materials reflects the ligating constraints imposed by the short tether length of the methylenediphosphonate ligand. While diphosphonates commonly possess sufficient spatial extension to bridge cluster building blocks, methylenediphosphonate is constrained by the short tether length to adopt chelation through oxygen donors at each phosphorus site as the preferential ligating mode. Consequently, the common $\{Mo_5O_{15}(O_3PR)_2\}^{4-}$ cluster will not be incorporated into materials incorporating methylenediphosphonate components.

As shown in Figure 6, the structure of $[\{Cu_2(tpypyz)(H_2O)_3\}Mo_5O_{15}(HPO_4)_2]\cdot 2H_2O$ (**5**·$2H_2O$) is two-dimensional. The network is constructed from $\{Mo_5O_{15}(HPO_4)_2\}^{4-}$ clusters employing three attachment points at terminal molybdenum oxo groups to link to Cu sites of three binuclear cationic components. While both crystallographically unique Cu(II) centers exhibit $\{CuN_3O_3\}$ 4 + 2 geometry, one site bridges two adjacent phosphomolybdate clusters and bonds to a single aqua ligand while the second Cu(II) site bonds to one

Table 2. Summary of Structural Characteristics for Materials of the Oxomolybdate (O_3ER)/Cu(II)/Organoimine Family, E = P and As

compound	overall dimensionality	Cu(II) component structure	copper molybdate substructure	phosphomolybdate substructure	ref
		Class 1: Isolated $\{MoO_6\}$ Octahedra			
$[Cu(bpy)(MoO_2)(H_2O)(O_3PCH_2PO_3)]$	1-D	$\{CuN_2O_3\}$ square pyramid	binuclear unit	$\{MoO_2(H_2O)(O_3PCH_2PO_3)\}_n^{2n-}$ chain	16
		Class 2: Bioctahedral Molybdate Unit			
$[Cu(phen)(Mo_2O_5)(H_2O)(O_3PCH_2PO_3)]$	1-D	$\{CuN_2O_3\}$ square pyramid	trinuclear unit	$\{(Mo_2O_5)(O_3PCH_2PO_3)]\}_n^{2n-}$ chain	15
$[Cu(terpy)(Mo_2O_5)(O_3PCH_2PO_3)]$	2-D	binuclear unit of edge-sharing square pyramids	no connectivity between Cu and Mo polyhedra	$\{(Mo_2O_5)(O_3PCH_2PO_3)\}_n^{2n-}$ chain	16
$[Cu(bpy)(Mo_2O_5)(O_3PCH_2CH_2CH_2PO_3)]$	2-D	$\{CuN_2O_4\}$ 4 + 2 octahedron	$\{Cu(bpy)(Mo_2O_5)\}_n^{4n+}$ chain	$\{(Mo_2O_5)(O_3PCH_2CH_2CH_2PO_3)\}_n^{2n-}$ network	16
$[Cu(bpy)(Mo_2O_5)(H_2O)(O_3PCH_2PO_3)]\cdot H_2O$	2-D	$\{CuN_2O_3\}$ square pyramid	trinuclear unit	$\{(Mo_2O_{15})(H_2O)(O_3PCH_2PO_3)\}_n^{3n-}$ network	16
		Class 3: Trioctahedral Molybdate			
$[\{Cu_2(tpyprz)(H_2O)(Mo_3O_8)(O_3PCH_2PO_3H)_2]\cdot 8H_2O$ (**3**·8H_2O)	1-D	$\{CuN_3O_2\}$ square pyramid	no connectivity between Cu and Mo polyhedra	$\{(Mo_3O_8)(O_3PCH_2PO_3H)_2\}^{4-}$ clusters	*a*
$[\{Cu_2(tpyprz)(H_2O)\}_2(Mo_3O_8)_2(O_3PCH_2PO_3)_3]\cdot 14.8H_2O$ (**4**·14.8H_2O)	1-D	$\{CuN_3O_2\}$ square pyramid	no connectivity between Cu and Mo polyhedra	$\{(Mo_3O_8)_2(O_3PCH_2PO)_3\}^{8-}$ cluster	*a*
		Class 4: Tetraoctahedral Molybdate Unit			
$[\{Cu(bpy)\}_2(Mo_4O_{12})(H_2O)_2(O_2PCH_2CH_2PO_3)]\cdot 2H_2O$	2-D	$\{CuN_2O_4\}$ 4 + 2 octahedron	$\{Cu(bpy)(Mo_4O_{12})(H_2O)_2\}_n^{4n+}$ chain	$\{(Mo_4O_{12})(H_2O)_2(O_3PCH_2CH_2PO_3)\}_n^{4n-}$ network	16
$[\{Cu(phen)\}_2(Mo_4O_{12})(H_2O)_2(O_3PCH_2CH_2PO_3)]\cdot 2H_2O$	2-D	$[CuN_2O_3]$ square pyramid	$\{Cu_2(phen)_2(Mo_4O_{12})\}X_n^{4n+}$ chain	$\{(Mo_4O_{12})(O_3PCH_2PO)\}_n^{4n-}$ chain	15
$[\{Cu(terpy)\}_2Mo_4O_{13}H(AsO_4)]\cdot 2H_2O$	1-D	$\{CuN_3O_2\}$ square pyramid	$\{Cu_2(terpy)_2Mo_4O_{13}H\}_n^{3n+}$ pentanuclear cluster	$\{Mo_4O_{13}H(AsO_4)\}^{4-}$ cluster	*b*
		Class 5: Pentaoctahedral Molybdate Unit			
$[\{Cu_2(tpypyz)(H_2O)\}(Mo_5O_{15})(O_3PC_6H_5)_2]\cdot 2H_2O$ (**2**·2H_2O)	1-D	$\{CuN_3O\}$ square plane and $\{CuN_3O_2\}$ square pyramid	$\{Cu(tpypyz)_{0.5}Mo_5O_{15}\}^{2+}$ cluster	$\{(MoO_{15})(O_3PC_6H_5)_2\}^{4-}$ cluster	*a*
$[\{Cu_2(tpypyz)(H_2O)\}(Mo_5O_{15})(O_3POH)_2]\cdot 2H_2O$	2-D	$\{CuN_3O_3\}$ 4 + 2 octahedron	$\{Cu_2(Mo_5O_{15})\}^{4+}$ network	$\{(Mo_5O_{15})(O_3POH)_2\}^{4-}$ cluster	14
$[\{Cu_2(tpypyz)(H_2O)_2\}(Mo_5O_{15})(O_3POH)_2]\cdot 3H_2O$	3-D	$\{CuN_3O_3\}$ 4 + 2 octahedron	$\{Cu_2(Mo_5O_{15})\}^{4+}$ chain	$\{(Mo_5O_{15})(O_3POH)_2\}^{4-}$ cluster	14
$[\{Cu(bpy)_2\}\{Cu(bpy)(H_2O)\}(Mo_5O_{15})(O_3PCH_2CH_2CH_2CH_2PO_3)]\cdot H_2O$	1-D	$\{CuN_4O\}$ and $\{Cu_2O_3\}$ square pyramids	$\{Cu_2(bpy)_3(H_2O)(Mo_5O_{15})\}^{4+}$ cluster	$\{(Mo_5O_{15})(O_3PCH_2CH_2CH_2CH_2PO_3)\}_n^{4n-}$ chain	13
$[\{Cu(phen)_2\{Cu(phen)(H_2O)_2\}(Mo_5O_{15})(O_3PCH_2CH_2CH_2PO_3)]\cdot 2.5H_2O$	1-D	$\{CuN_4O\}$ and $\{CuN_2O_3\}$ square pyramids	$\{Cu_2(phen)_3(H_2O)_2(Mo_5O_{15})\}^{4+}$ cluster	$\{(Mo_5O_{15})(O_3PCH_2CH_2CH_2PO_3)\}_n^{4n-}$ chain	15
$[\{Cu(terpy)(H_2O)\}_2(Mo_5O_{15})(O_3PCH_2CH_2PO_3)]\cdot H_2O$	1-D	$\{CuN_3O_2\}$ square pyramid	$\{Cu_2(terpy)_2(Mo_2O_{15})\}^{4+}$ cluster	$\{(Mo_5O_{15})(O_3PCH_2CH_2PO_3)\}_n^{4n-}$ chain	16
$[\{Cu(terpy)\}_2(Mo_5O_{15})(O_3PCH_2CH_2CH_2PO_3]$	2-D	$\{CuN_3O_2\}$ square pyramid	$\{Cu_2(terpy)_2(Mo_5O_{15})\}_n^{4n+}$ chain	$\{(Mo_5O_{15})(O_3PCH_2CH_2CH_2PO_3)\}_n^{4n-}$chain	16
$[\{Cu_2(tpypyz)(H_2O)_2\}(Mo_5O_{15})(O_3PCH_2CH_2PO_3)]\cdot 5.5H_2O$	2-D	$\{CuN_3O_2\}$ square pyramid and $\{CuN_3O_3\}$ 4 + 2 octahedron	$\{Cu_2(terpy)(H_2O)_2(Mo_5O_{15})\}_n^{4n+}$ chains	$\{(Mo_5O_{15})(O_3PCH_2CH_2CH_2PO_3\}_n^{4n-}$ chain	13
$[\{Cu_2(tpypyz)(H_2O)_3\}(Mo_5O_{15})(HPO_4)(O_3PCH_2CO_2H)]\cdot H_2O$ (**1**·H_2O)	1-D	$\{CuN_3O_2\}$ square pyramid and $\{CuN_3O_3\}$ 4 + 2 octahedra	$\{Cu_2(tpypyz)Mo_5O_{15}\}_n^{4n+}$ chains	$\{Mo_5O_{15}(HPO_4)(O_3PCH_2CO_2H)\}^{4-}$ cluster	*a*
$[\{Cu_2(tpypyz)(H_2O)_3\}(Mo_5O_{15})(HPO_4)_2]\cdot 2H_2O$ (**5**·2H_2O)	2-D	$\{CuN_3O_3\}$ 4 +2 octahedron	$\{Cu_2(tpypyz)Mo_5O_{15}\}_n^{4n+}$ 2-D network	$\{Mo_5O_{15}(HPO_4)_2\}^{4-}$ cluster	*a*
$[\{Cu_2(tpypyz)(H_2O)_2\}(Mo_5O_{15})\{O_3P(CH_2)_nPO_3\}]\cdot xH_2O$ n = 3,4 (**6** and **7**)	3-D	$\{CuN_3O_3\}$ 4 + 2 octahedra	$\{Cu_2(tpypyz)Mo_5O_{15}\}_n^{4n+}$ 2-D network	$\{Mo_5O_{15}\{O_3P(CH_2)_nPO_3)\}^{4-}$ cluster	*a*
		Class 6: Hexaoctahedral Molybdate Unit			
$[\{Cu(o\text{-}phen)(H_2O)_2\}_2(O_3AsOH)_2]$	1-D	$\{CuN_2O_4\}$ 4 + 2 octahedron	$\{Cu_2(phen)_2(Mo_6O_{18})\}_n^{4n+}$ chains	unpublished results	
$[\{Cu_2(tpypyz)\}(Mo_6O_{18})(O_3AsR_5)_2]$ R = OH, C_6H_5	2-D	$\{CuN_3O_3\}$ 4 + 2 octahedron	$\{Cu_2(tpypyz)(Mo_6O_{18})\}_n^{4n+}$ network	$\{(Mo_6O_{18})(O_3AsC_6H_5)_2\}^{4-}$ cluster	*b*
$[\{Cu(LL)(H_2O)\}_2(Mo_6O_{18})(O_3AsC_6H_5)_2]\cdot 2H_2O$ (LL = 2,2′-bpy, *o*-phen)	1-D	$\{CuN_2O_4\}$ 4 + 2 octahedron	$\{Cu_2(LL)_2(Mo_6O_{18})\}_n^{4n+}$ chains	$\{(Mo_6O_{18}(O_3AsC_6H_5)_2\}^{4-}$ cluster	*b*

[a] This work. [b] Unpublished results.

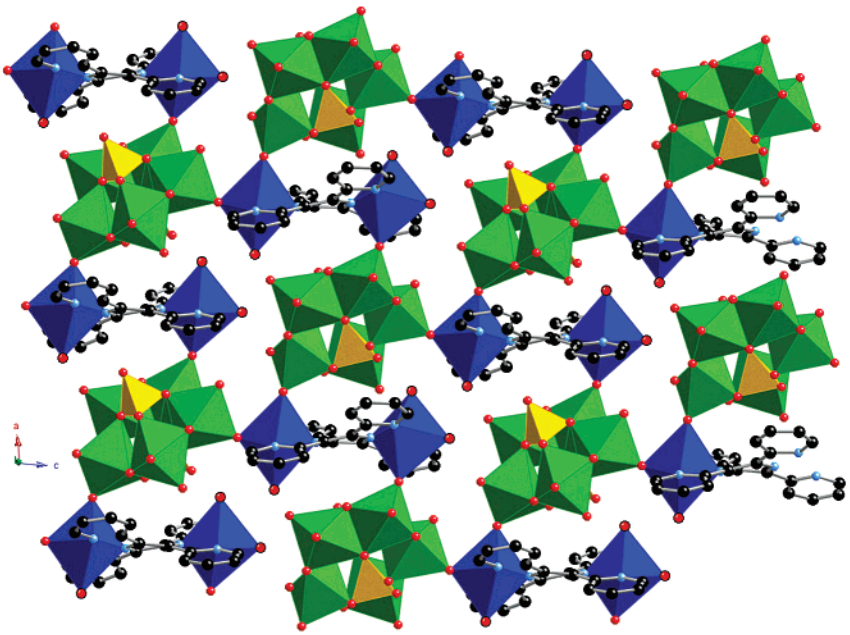

Figure 6. A view of the two-dimensional structure of $[\{Cu_2(tpypyz)(H_2O)_3\}Mo_5O_{15}(HPO_4)_2]\cdot 2H_2O$ (**5**·$2H_2O$).

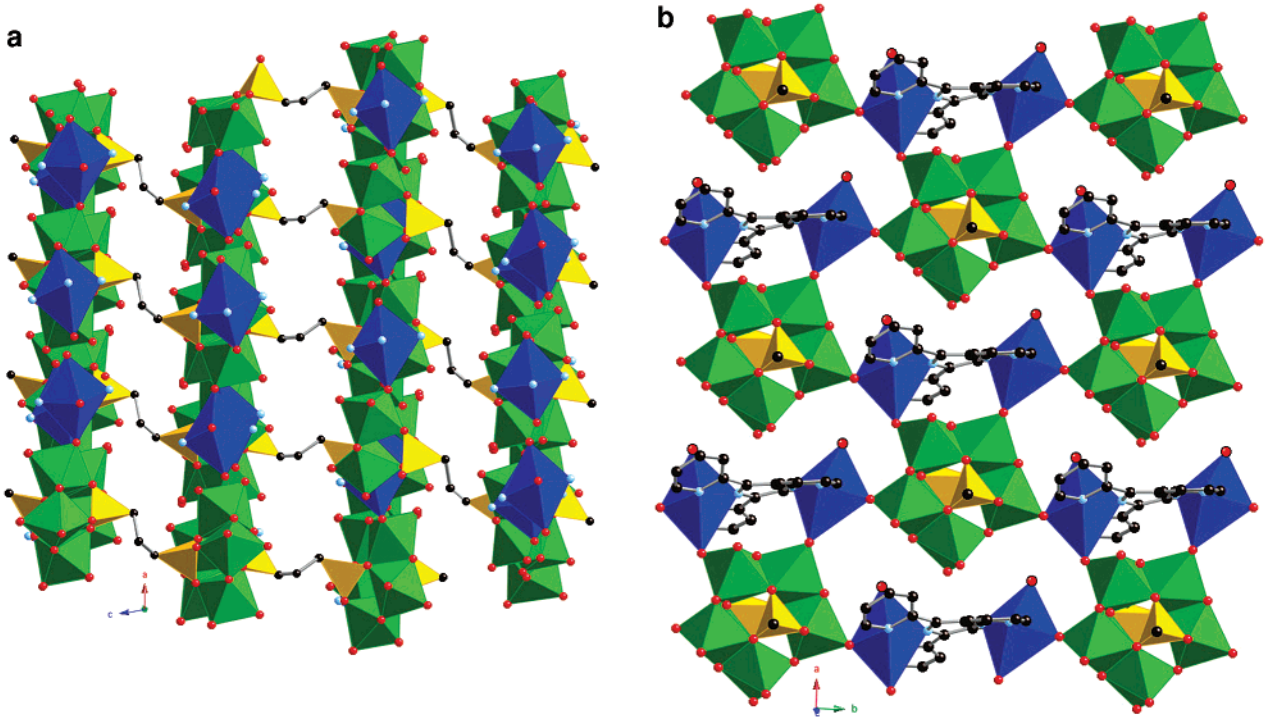

Figure 7. (a) A view of the three-dimensional structure of $[\{Cu_2(tpypyz)(H_2O)_2\}Mo_5O_{15}(O_3P(CH_2)_3PO_3\}]\cdot 2.25H_2O$ (**6**·$2.25H_2O$). (b) The copper molybdophosphonate two-dimensional substructure in the *ab* plane.

bridging oxo group and two aqua ligands. Consequently, each binuclear subunit bridges three phosphomolybdate clusters in forming the network architecture in the *ac* plane.

The structure of **5** may be compared to those of the previously reported[14] $[\{Cu_2(tpypyz)(H_2O)_2\}Mo_5O_{15}(HPO_4)_2]\cdot 2H_2O$ and $[\{Cu_2(tpypyz)(H_2O)_2\}Mo_5O_{15}(HPO_4)_2]\cdot 3H_2O$. The dihydrate is also two-dimensional, but in contrast to **5**, each phosphomolybdate cluster exhibits four oxo-bridge points of attachment to three neighboring binuclear subunits. Consequently, the 4 + 2 Cu(II) sites exhibit identical geometries: three nitrogen donors, two bridging oxo-groups from adjacent molybdate clusters, and one aqua ligand. In contrast, the trihydrate is three-dimensional, constructed of $\{Cu_2Mo_5O_{15}(HPO_4)_2\}$ chains, and linked through the tpypyz groups into a framework structure. The expanded dimensionality of the trihydrate is consequently a reflection of the orientation of the $\{Cu_2(tpypyz)(H_2O)_2\}^{2+}$ subunits with respect to the direction of propagation of $\{Cu_2Mo_5O_{15}(HPO_4)_2\}$ chain substructure.

The structures of $[\{Cu_2(tpypyz)(H_2O)_2\}Mo_5O_{15}\{O_3P(CH_2)_3PO_3\}]\cdot 2.25H_2O$ (**6**·$2.25H_2O$) and $[\{Cu_2(tpypyz)(H_2O)_2\}Mo_5O_{15}\{O_3P(CH_2)_4PO_3\}]\cdot 0.33H_2O$ (**7**·$0.33H_2O$) are three-

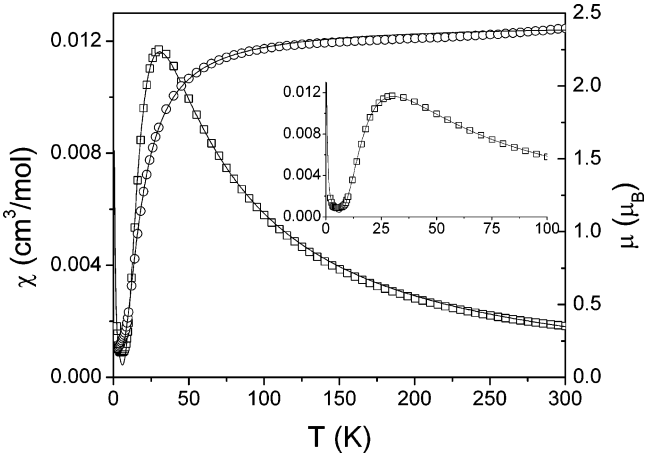

Figure 8. The dependence of magnetic susceptibility χ of [{Cu_2(tpypyz)-(H_2O)$_2$}Mo_5O_{15}{$O_3P(CH_2)_3PO_3$}]·2.25H_2O (**6**·2.25H_2O) with temperature *T*. The line drawn through the data is the fit to the Heisenberg dimer model.

dimensional. As shown in Figure 7, the architecture is constructed from networks of $\{Mo_5O_{15}(O_3PR)_2\}^{4-}$ clusters linked through $\{Cu_2(tpypyz)(H_2O)_2\}^{4+}$ subunits in the *ab* plane, which are tethered through alkyl chains running parallel to the *c* axis. The network structure is that of [{Cu_2(tpypyz)(H_2O)$_2$}$Mo_5O_{15}(HPO_4)_2$]·2H_2O rather than that of **5**·2H_2O. Thus, each phosphomolybdate cluster exhibits four attachment points to the Cu subunits, while each 4 + 2 Cu site bridges two clusters. The interlamellar distances reflect the tether lengths: ca. 8.0 Å for **6** and 8.5 Å for **7**.

Magnetism. Since the molybdenum(VI)−organophosphonate substructures of the compounds are diamagnetic, the paramagnetism of the materials is a consequence of the presence of the d^9-Cu(II) sites. The magnetism of the representative compounds **1** and **3**−**7** all exhibit maxima in the χ vs *T* plots in the 30−40 K range, as illustrated in Figure 8 for **6**. The data are consistent with the presence of antiferromagnetic interactions between Cu(II) sites.

The best description of the experimental results have been obtained using the Heisenberg dimer model for two $S = {}^1/_2$ Cu(II) sites:

$$\chi = (1-x)\frac{N_A g^2 \mu_B^2}{k_B T}\frac{2\exp\left(\frac{2J}{k_B T}\right)}{1+3\exp\left(\frac{2J}{k_B T}\right)} + x\frac{N_A g^2 \mu_B^2}{2k_B T} + TI \quad (1)$$

The best fit was $g = 2.06$, $J/k_B = -27.5$ K, $TI = -0.00055$ cm^3/mol, $x = 0.011$ for **1**; $g = 2.10$, $J/k_B = 25.5$ K, $TI = -0.00062$, $x = 0.007$ for **3**; $g = 2.14$, $J/k_B = -28.0$ K, $TI = -0.00081$ cm^3/mol, $x = 0.009$ for **4**; $g = 1.93$, $J/k_B = -29.5$ K, $TI = -0.00063$ cm3/mol, $x = 0.07$ for **5**; $g = 1.99$, $J/K_B = -24.7$ K, $TI = 0.00056$ cm^3/mol, $x = 0.008$ for **6**; and $g = 2.12$, $J/k_B = -30.5$ K, $TI = 0.00035$ cm^3/mol, $x = 0.0003$ for **7**. The similarities in the plot profiles and in the fit parameters indicate that the weak antiferromagnetism (J/k_B: −24.7 to −30.5 K) results from the same interaction in all cases, suggesting that the Cu(II) sites communicate through the planar, π-delocalized tpypyz ligands in the $\{Cu_2(tpypyz)(H_2O)_x\}^{4+}$ binuclear subunits.[26] The effective moments at 300 K for **1**−**7** fall in the range of 2.30−2.65 μ_B, compared to a calculated value of 2.79 μ_B for two noninteracting Cu(II) ions.

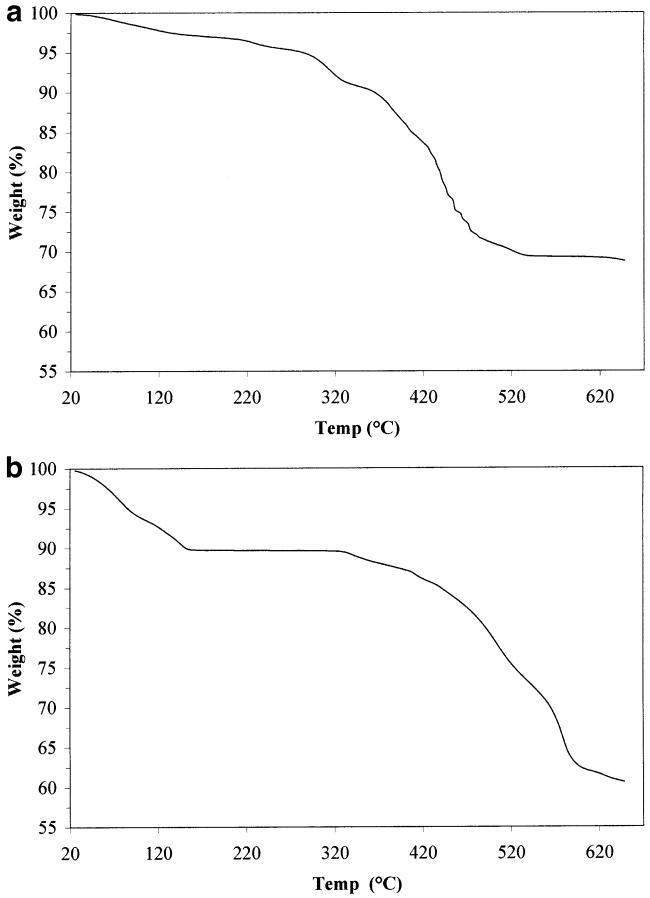

Figure 9. TGA curves for the thermal decompositions of (a) [{Cu_2(tpyprz)-(H_2O)$_3$}$Mo_5O_{15}(HPO_4)(O_3PCH_2CO_2H)$]·$H_2O$ (**1**·H_2O) and (b) [{Cu_2(tpyprz)-(H_2O)}$_2$(Mo_3O_8)$_2$($O_3PCH_2PO_3$)$_3$]·14.8H_2O (**4**·14.8H_2O).

Thermal Behavior. In general, the thermal decompositions of the compounds of this study are characterized by the loss of water of crystallization at temperatures below 150 °C and organic and aqua ligand loss above 250 °C. As shown in Figure 9a, compound **1** exhibits gradual dehydration in the room temperature to 250 °C range, accounting for a 4.8% weight loss, attributed to the loss of the water of crystallization and the three aqua ligands associated with the Cu(II) sites (4.7% theoretical). This process is followed by a weight loss of ca. 27.0%, attributed to ligand decomposition in the 300−500 °C range (27.1% theoretical). The final product is a mixture of P_2O_5, $CuMoO_4$, and amorphous material.

In the case of **4**·16.9H_2O (Figure 9b), the dehydration process starts at room temperature and loss of water of crystallization is complete by 120 °C (10.0% weight loss calculated for 14.8H_2O; 10.2% observed). The initial weight loss is followed by a plateau (125−315 °C), whereupon the aqua groups and the ligand are released in the 318−590 °C range to give a mixture of P_2O_5, $CuMoO_4$, and MoO_3. It is noteworthy that the water of crystallization of **4** is released at temperatures below 125 °C, indicating that the channels within the crystal structure are readily accessible to the water

(26) Koo, B.-K.; Bewley, L.; Golub, V.; Rarig, R. S.; Burkholder, E.; O'Connor, C. J.; Zubieta, J. *Inorg. Chim. Acta*, in press.

molecules,[27] an observation consistent with the structure of **4** described above. Furthermore, the coordinated aqua groups are not released below 320 °C as they are bound to Cu(II) sites and in environments relatively inaccessible to the pore structure of the material. This is a consistent feature of the thermal characteristics of all compounds of this study, which in no case exhibit loss of aqua ligands below 250 °C.

Conclusions

The structures of this study demonstrate the persistence of the $\{Mo_5O_{15}(O_3PR)_2\}^{4-}$ core as a building block for extended structures under the conditions of synthesis. In fact, there are now nearly 20 reported structures constructed through the expedient linking of $\{Mo_5O_{15}(O_3PR)_2\}^{4-}$ or $\{Mo_6O_{18}(O_3AsR)_2\}^{4-}$ clusters, as summarized in Table 2. The dimensionality of these materials is to some extent controllable by manipulation of the component building blocks. However, it is also apparent that the number of attachment points on the clusters is variable and not readily predictable for a particular set of reaction conditions. Thus, for the cationic molecular subunit $\{Cu_2(tpypyz)(H_2O)_n\}^{4+}$, two, three, and four sites may be available on the surface of the phosphomolybdate cluster, allowing structural extension in one-, two-, or three-dimensions.

It is also noteworthy that considerable structural variation is possible at the Cu(II) site which may adopt square planar, $4 + 1$, or $4 + 2$ coordination modes. Different coordination sites may arise in a given material. Likewise, the extent of aqua coordination at the Cu(II) sites may vary even within a single binuclear substructure.

The most pronounced structural anomalies in this family of materials occurs upon introduction of methylenediphosphonate as the tethering ligand. As noted above, the distinctive coordination properties of methylenediphosphonate preclude the incorporation of $\{Mo_5O_{15}(O_3PR)_2\}^{4-}$ clusters into the solid and give rise to the unique structural chemistry summarized in Table 2.

Curiously, the ethylenediphosphonate building block under conditions that would favor isolation of the pentamolybdate cluster does so with terpyridine and tetra-2-pyridylpyrazine as ligands to copper in $[\{Cu(terpy)(H_2O)\}_2Mo_5O_{15}(O_3PCH_2CH_2PO_3)]$ and $[\{Cu_2(tpypyz)(H_2O)_2\}Mo_5O_{18}(O_3PCH_2CH_2PO_3)]$ but results in incorporation of the $\{Mo_4O_{12}(H_2O)_2(O_3PR)_2\}^{4-}$ cluster with bpy and phen as ligands in $[\{Cu(LL)\}_2Mo_4O_{12}(H_2O)_2(O_3PCH_2CH_2PO_3)]$ (LL = bpy or phen). These latter structures feature P−O−Cu bridging oxygen donors as well as Mo−O−Cu bridges. Furthermore, the aqua ligands are associated with the Mo sites. While P−O−Cu bonding is common for the chelating methylenediphosphonate ligand, it occurs much less frequently with larger spaces ($n = 2, 3, 4$). However, three of the four instances of this bonding type with $n > 1$ occur with ethylenediphosphonate ligation, suggesting that tether length remains a determinant in these cases.

We conclude that, while under reaction conditions favoring the self-assembly of $\{Mo_5O_{15}(O_3PR)_2\}^{4-}$ clusters, a molecular building block approach to oxide materials has been established, the dynamic nature of the hydrothermal reaction domain and the structural versatility of the component substructures render absolute structural predictability problematic. As the structural database for these materials expands and the hydrothermal reaction space is more fully explored, it is anticipated that the structure−reaction correlations will continue to emerge.

Acknowledgment. This work was supported by a grant from the National Science Foundation, CHE-0242153.

Supporting Information Available: Tables of bond lengths, bond angles, anisotropic temperature factors, and atomic positional parameters for **1**−**7** in CIF format. This material is available free of charge via the Internet at http://pubs.acs.org.

IC030169O

(27) Petit, S.; Coquerel, G. *Chem. Mater.* **1996**, *8*, 2247.